Speed of Intersubunit Communication in Proteins

Colleen M. Jones, Anjum Ansari, Eric R. Henry, Garrott W. Christoph, James Hofrichter,* and William A. Eaton*

Laboratory of Chemical Physics, Building 2, National Institute of Diabetes and Digestive and Kidney Diseases, National Institutes of Health, Bethesda, Maryland 20892

Received February 21, 1992; Revised Manuscript Received April 21, 1992

ABSTRACT: To determine the speed of communication between protein subunits, time-resolved absorption spectra were measured following partial photodissociation of the carbon monoxide complex of hemoglobin. The experiments were carried out using linearly polarized, 10-ns laser pulses, with the polarization of the excitation pulse both parallel and perpendicular to the polarization of the probe pulse. The substantial contribution to the observed spectra from photoselection effects was eliminated by isotropically averaging the polarized spectra, allowing a detailed comparison of the kinetics as a function of the degree of photolysis. These results show that prior to 1 μs both geminate ligand rebinding and conformational relaxation are independent of the number of ligands dissociated from the hemoglobin tetramer, as expected for a two-state allosteric model. After this time the kinetics depend on the ligation state of the tetramer. The conformational relaxation at 10 μs can be interpreted in terms of the two-state allosteric model as arising from the R to T quaternary conformational change of both unliganded and singly liganded molecules. These results suggest that communication between subunits requires about 1 μs and that the mechanism of the communication which occurs after this time is via the R to T conformational change. The optical anisotropy provides a novel means of accurately determining the extinction coefficients of the transient photoproduct. The decay in the optical anisotropy, moreover, provides an accurate determination of the rotational correlation time of 36 $\pm$ 3 ns.

Laser photolysis of hemoglobin provides a unique opportunity to investigate the dynamics of the interaction between protein subunits. In these experiments a short laser pulse is used to photodissociate one or more ligands from the carbonmonoxyhemoglobin tetramer, and the subsequent events are monitored by time-resolved optical absorption spectroscopy. Within 300 ns about 40% of the photodissociated ligands geminately rebind to the heme at room temperature; the remainder escape into the solvent and may rebind in a bimolecular process (Duddell et al., 1979; Alpert et al., 1979; Friedman & Lyons, 1980; Hofrichter et al., 1983). Spectral changes of the deoxyheme occur simultaneously with geminate rebinding, indicating evolution of the protein conformation toward that of deoxyhemoglobin at equilibrium (Lyons & Friedman, 1982; Hofrichter et al., 1983, 1985, 1991; Friedman, 1985; Sassaroli & Rousseau, 1987; Murray et al., 1988a,b). Both the kinetics of geminate rebinding and the kinetics of the deoxyheme spectral changes can be used as probes of subunit interaction. In this work we address two important questions concerning the dynamics of subunit interaction. First, how long does it take for the heme of one subunit of hemoglobin to respond to photodissociation of the heme complex on a neighboring subunit? That is, how fast is communication between subunits? Second, what is the mechanism of this communication?

To examine these questions we carried out a series of partial photolysis experiments on human hemoglobin in the R quaternary conformation using linearly polarized, 10-ns laser pulses. By varying the degree of photolysis, the distribution of tetramers having different numbers of photodissociated heme complexes was varied. The resulting kinetics were then compared in a model-independent analysis to determine when differences began to appear and in a model-dependent analysis to determine how the kinetics of the quaternary conformational change depend on the number of ligands bound. Since hemoglobin in the T quaternary conformation shows less than 1% geminate rebinding (Murray et al., 1988a), the geminate kinetics for hemoglobin initially in the R conformation, but evolving toward the T conformation following ligand photodissociation, provide a sensitive measure of communication between subunits.

Previous nanosecond experimental studies on trout hemoglobin suggested that photoselection effects have a major influence on measurements of geminate rebinding because rotational diffusion of hemoglobin occurs on the same time scale (Hofrichter et al., 1991). A theoretical analysis also showed that photoselection effects are significant even at degrees of photolysis greater than 90% (Hofrichter et al., 1991; Ansari and Szabo, in preparation; Ansari et al., in preparation). By making measurements with the probe pulse polarized both parallel and perpendicular to the photolysis pulse, we could obtain isotropically averaged spectra which contained no interference from photoselection effects. There were additional advantages in making the measurements with both polarizations. The optical anisotropy induced in the sample provided information on the reorientational dynamics of the heme group in addition to that due to the overall rotation of the protein. The measurement of the optical anisotropy, moreover, together with the theory of Ansari and Szabo (in preparation), provided a novel method for accurately determining the extinction coefficients of the photoproduct spectra and therefore for accurately determining the degree of photolysis.

MATERIALS AND METHODS

Sample Preparation. A lysate of human red cells was prepared from freshly drawn blood following the method of Perutz (1968). Oxyhemoglobin A was purified by DEAE-Sephacel (Pharmacia) anion-exchange chromatography using a pH gradient between 8.5 and 7.8 in 0.05 M Tris-HCl[1]

* Correspondence should be addressed to either of these authors.

(Schroeder & Huisman, 1980). After concentration by ultrafiltration (Amicon) and vacuum dialysis against 0.1 M potassium phosphate (pH 7.0), the purified oxyhemoglobin A was stored in liquid nitrogen as beads.

The carbonmonoxyhemoglobin (HbCO) sample for the photolysis experiments was prepared by diluting the thawed beads into 0.1 M potassium phosphate buffer (pH 7.0), equilibrating the diluted solution with water-saturated carbon monoxide (CO), and loading the solution into a CO-purged cuvette (Wilmad WG-814 EPR flat cell). The solution contained 8 mM sodium dithionite to remove any traces of oxygen. The ends of the cell were sealed with dental wax and Glyptal varnish to maintain anaerobic conditions. The data reported here were obtained from two samples of different concentrations but almost the same optical densities. In one the heme concentration was 120 μM and the path length was 360 μm, while in the other the heme concentration was 950 μM and the path length was 48 μm. Unless stated otherwise, the data presented in the figures will be those from the 120 μM sample.

Instrumentation. The transient absorption laser spectrometer used in these experiments is the same as that described previously (Hofrichter et al., 1991). The second harmonic (532 nm, 10-ns pulse width, fwhm) of a Q-switched Nd:YAG laser (Quanta-Ray/Spectra-Physics DCR-1A) was used to photolyze the HbCO complex. The third harmonic (355 nm) of a second Q-switched Nd:YAG laser (Quanta-Ray/Spectra-Physics DCR-1) was used to excite the fluorescence of a stilbene 420/methanol solution which was pumped through quartz capillary tubing. The dye emission, which spans a wavelength range of 390–480 nm, acted as a broad-band probe source which could be temporally delayed from the photolysis beam by electronically adjusting the time interval between the firing of the two lasers. Slit-shaped images of the photolysis and probe beams were focused onto the sample such that the spatial profile of the photolysis beam overfilled the width of only the bottom half of the probe image. The image at the sample was then focused at the 100-μm entrance slit of a 1/4 meter monochromator. The dispersed image of the slit was focused onto two tracks of a silicon target vidicon detector (EG&G PAR Model 1252E); the photolyzed region of the image filled one of the tracks and the unphotolyzed region filled the second track. Photoproduct minus HbCO difference spectra were calculated from the logarithm of the ratio of intensities in the photolyzed and unphotolyzed tracks. A detector controller (EG&G PAR Model 1216), directed by a Hewlett-Packard 9826 desktop calculator, was used to collect the data. The calculator also controlled the laser firing and synchronization as well as data averaging.

Each measured spectrum derived from the summed intensities accumulated over 45 laser shots. A Glan-Laser polarizing prism (Melles Griot) with an extinction ratio of $<5 \times 10^{-5}$ ensured the purity of the linear polarization of the photolysis beam. The polarization direction of the 532-nm beam was controlled by rotation of a $\lambda/2$ waveplate. A dichroic sheet polarizer positioned after the dye cell was used to polarize the probe source. The extinction ratio of the probe light, measured by placing a polarization analyzer at the sample, was 0.005. The intensity of the photolysis beam in the partial photodissociation experiments was modulated by adjusting the laser lamp energy and/or by insertion of neutral density filters (Rolyn) into the beam path. The sample was maintained at 20 ± 0.2 °C by a recirculating bath (Neslab Model RTE-110) and a specially constructed copper block connected to a brass heat transfer block/thermocouple assembly encasing the sample. To minimize temperature gradients, nitrogen equilibrated at the temperature of the block was passed over the exposed surface of the sample cuvette.

Data Analysis. The data consists of sets of difference spectra measured at logarithmically-spaced time intervals ranging from about 20 ns prior to the photolysis pulse to about 80 ms after the pulse, for pulse energies which produced between about 10% and 95% photolysis. Data at 16 levels of photolysis for the 120 μM sample and 21 degrees of photolysis for the 950 μM sample were obtained with the electric vector of the linearly polarized photolysis pulse aligned both parallel and perpendicular to that of the probe pulse. All of the data at a single concentration were simultaneously analyzed using a slightly modified form of a singular value decomposition procedure (SVD) previously described by Hofrichter et al. (1991). Since the spectral resolution is determined by the 100-μm slit width of the monochromator and the width of a single pixel is 25 μm, the data were smoothed over 4 pixels using a Gaussian filter with a fwhm of 2 pixels to reflect this resolution. After being smoothed, the polarized difference spectra at all times and levels of photolysis were linearly interpolated onto a common wavelength grid spaced at 1-nm intervals. The data were also mapped onto a standard time delay grid by linear interpolation after the initial times of the kinetic traces were determined for each experiment; the interpolation affected data only within the first few hundred nanoseconds since the grid was chosen to coincide with the measured data at the longer time delays. To temporally align the data, the ligand rebinding curves from about 20 ns prior to the photolysis pulse to about 70 ns after the photolysis pulse were averaged using SVD and the deviations of the individual curves from the average kinetic trace were minimized. Simulations in which the photolysis and probe pulses were modeled as Gaussians (fwhm = 10 ns) have shown that the time at which the absorption signal maximizes does not correspond to the time where there is maximum temporal overlap between the photolysis and probe pulses (Ansari et al., in preparation). The point at which the absorption signal maximizes depends on the short-time kinetics of the system and on the incident laser intensity. On the basis of these simulations we assigned our initial point to 10 ns. After alignment, the data prior to 10 ns were discarded.

The data were then assembled into a global data matrix, **D**, which consisted of difference optical densities measured as a function of four variables: the wavelength of the probe beam, the time delay between the photolysis and probe beams, the degree of photolysis, and the relative polarization directions for the electric field vectors of the photolysis and probe beams. The singular value decomposition of **D** can be written as

$$\mathbf{D} = \mathbf{USV}^{\mathrm{T}} \quad (1)$$

where the columns of **U** are a set of linearly independent, orthonormal basis spectra, the columns of **V** describe the time-, polarization-, and photolysis-dependent amplitudes of these basis spectra, and the matrix **S** is a diagonal matrix of nonnegative singular values which describe the magnitudes of the contributions of each of the outer products of the ith column vectors $U_iV_i^{\mathrm{T}}$ to the data matrix **D** (Henry & Hofrichter, 1992).

Since most of the higher order components of the SVD contain no real spectral information and correspond to noise with a random time dependence, only the twelve components with the highest singular values were retained for further

[1] Abbreviations: CO, carbon monoxide; DEAE, diethylaminoethyl; deoxyHb, deoxyhemoglobin; fwhm, full width at half maximum; Hb, hemoglobin; HbCO, carbonmonoxyhemoglobin; OD, optical density; SVD, singular value decomposition; Tris, tris(hydroxymethyl)aminomethane.

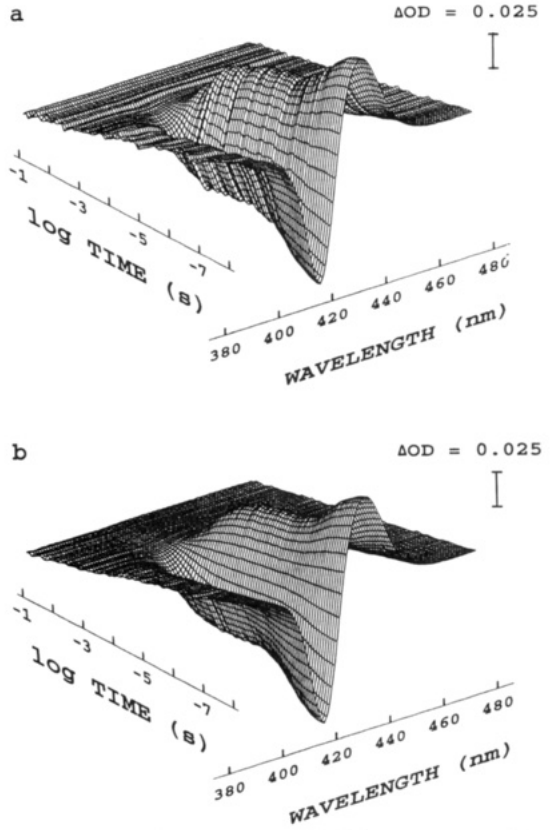

FIGURE 1: Photoproduct minus HbCO difference spectra following 22% photolysis. Difference optical densities are shown at 1-nm intervals for spectra measured at 89 time delays between firing the photolysis and probe lasers. (a) Spectra after smoothing to reflect the spectrometer resolution but prior to removal of baseline offsets. (b) Spectra after smoothing and removal of baseline offsets according to the procedure described in the text.

analysis. The primary source of noise in our data is from baseline offsets which derive from shot-to-shot variations in the probe laser intensity and have a random time dependence. The offset appeared mainly in the third basis spectrum (U_3). Due to the orthogonality constraint of the SVD procedure, the third basis spectrum (not shown) was not a pure offset spectrum but was mixed to a small extent with other wavelength-correlated experimental artifacts, as well as with contributions from real spectral changes. The rotation procedure described by Henry and Hofrichter (1992) and used by Hofrichter et al. (1991) to discriminate against such random sources of experimental noise was not used in the current analysis. We developed an alternative procedure to extract a pure offset component from the data. The baseline offset was assumed to be a constant optical density difference at every wavelength. The third basis spectrum was expressed as a linear combination of a pure offset (U_0) plus the remaining 11 basis spectra, with the coefficients determined by a least-squares fit, i.e.

$$s_3 U_3 \cong c_0 U_0 + \sum_{i \neq 3} c_i s_i U_i \qquad (2)$$

where s_i is the singular value of the ith component and where the sum extends over the first 12 SVD components. After the pure offset term, $c_0 U_0 V_3^T$, is discarded, the data matrix can be written

$$\mathbf{D} \cong \sum_{i \neq 3} s_i U_i (V_i^T + c_i V_3^T) \qquad (3)$$

In this data matrix the largest random fluctuations originally associated with the offset have been removed. Figure 1 illustrates the effectiveness of this procedure.

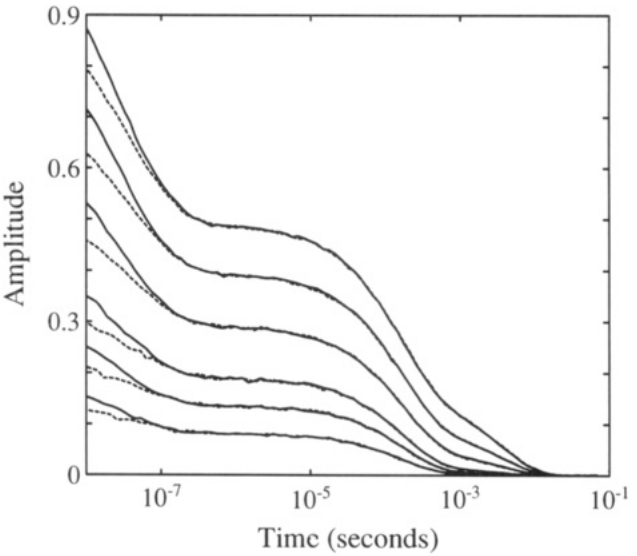

FIGURE 2: Ligand rebinding curves at various degrees of photolysis prior to correction for photoselection effects. The first column of the **V** matrix (V_1) obtained from the singular value decomposition of the data matrix **D** (eq 3) is plotted as a function of the time delay between the photolysis and probe pulses. The continuous curves correspond to experiments with the parallel orientation of the electric vectors of the photolysis and probe pulses, while the dashed curves correspond to those with the perpendicular orientation. The degrees of photolysis were 13%, 22%, 31%, 48%, 65%, and 81% as determined from the data in Figure 3; the curves have been scaled to reproduce these values.

To calculate linear dichroism spectra and isotropically averaged spectra, it was first necessary to correct for small differences in the degree of photolysis for each polarization. Differences in excitation laser energy arise when the polarization of the photolysis beam is rotated by 90° because of differential reflection losses at the sample cuvette surface (which is oriented at an angle relative to the propagation direction) and from slow changes in laser intensity arising from drifts in the beam position. The correction procedure is based on the result discussed below that at all degrees of photolysis the spectra in both polarizations at each time delay in the time range 200 ns to 1 μs are proportional to within a scale factor. At times less than 200 ns the spectra differ because of photoselection effects, while at times longer than 1 μs the kinetics depend on the degree of photolysis. Differences in the optical densities measured during the 200 ns–1 μs time window reflect differences in the extent of photolysis. To correct the data, the optical densities measured at time delays within this range were first averaged to determine the photolysis level for each polarization. The observed photolysis-dependent optical densities at a given time delay and wavelength for the polarized data were then linearly interpolated to the same photolysis level.

RESULTS

The time-resolved spectra (Figure 1b) reported in this study consist of photoproduct minus HbCO difference spectra at various time delays following partial photodissociation with linearly polarized 10-ns (fwhm) laser pulses. To exploit and eliminate photoselection effects, spectra were measured with both parallel and perpendicular orientations of the electric vector of the probe beam relative to that of the photolysis beam. For each degree of photolysis, spectra were obtained at 89 time delays between about 10 ns and 70 ms. The degree of photolysis ranged from about 10% to 80% for the 120 μM sample and from about 10% to 95% for the 950 μM sample. The curves in Figure 2 show the time course of the overall

amplitude of the spectra for each polarization at several degrees of photolysis. These curves represent a good first approximation to the ligand rebinding curves (Hofrichter et al., 1983, 1985, 1991; Murray et al., 1988a,b; Henry & Hofrichter, 1992). More precisely, these curves are the time course of the amplitude (V_1) of the first component (U_1) of the singular value decomposition of the data for each set of conditions. After about 200 ns the curves for both polarizations at each degree of photolysis are superimposable. Prior to 200 ns they differ because of the effects of photoselection and rotational diffusion.

Optical Anisotropy. To examine the photoselection effects in more detail, we calculated the average optical anisotropy as a function of time from the linear dichroism and the isotropic spectra. The linear dichroism ($\equiv\Delta OD_{\parallel} - \Delta OD_{\perp}$) decays because of both geminate rebinding of CO and randomization of the molecular orientations of the photoselected population by rotational diffusion. The contribution of the latter can be obtained from the optical anisotropy, $r(\lambda,t)$, defined at each wavelength (λ) and time delay (t) as

$$r(\lambda, t) \equiv \frac{\Delta OD_{\parallel}(\lambda, t) - \Delta OD_{\perp}(\lambda, t)}{\Delta OD_{\parallel}(\lambda, t) + 2\Delta OD_{\perp}(\lambda, t)} \quad (4)$$

The isotropic optical density difference, $\Delta OD_{iso}(\lambda, t)$, is given by

$$\Delta OD_{iso}(\lambda, t) = \frac{1}{3}[\Delta OD_{\parallel}(\lambda, t) + 2\Delta OD_{\perp}(\lambda, t)] \quad (5)$$

Since the noise in the anisotropy is large at wavelengths where the measured optical density in the isotropic spectrum is small, we used the square of the isotropic optical density difference to weight the anisotropy at each wavelength to calculate the average anisotropy at each time delay, $\bar{r}(t)$, i.e.

$$\bar{r}(t) = \frac{\sum_{\lambda} r(\lambda, t)[\Delta OD_{iso}(\lambda, t)]^2}{\sum_{\lambda} [\Delta OD_{iso}(\lambda, t)]^2} \quad (6)$$

Figure 3a shows representative decay curves for the average anisotropy at several degrees of photolysis. The curves at all levels of photolysis were fitted with a single exponential and yielded a time constant of 36 ± 3 ns. Figure 3b shows the first basis curve obtained in a singular value decomposition of the entire set of anisotropy decay curves at all levels of photolysis. The signal-to-noise is improved over that of the individual decay curves in Figure 3a, since this basis curve represents data averaged over the 16 measured levels of photolysis. An exponential fit to this single decay curve yields a time constant of 35 ns. The same analysis for the 950 μM sample gave a time constant of 35 ± 6 ns from the individual fits and 37 ns from the SVD, indicating that dissociation of tetramers into dimers is not having a major effect on this result.

Figure 3c shows the experimentally measured average anisotropy at 10 ns for both the 120 μM and 950 μM samples plotted as a function of the isotropic spectral amplitude of the photoproduct. These values were compared with theoretical results for a circular absorber by calculating the anisotropy at the end of a square pulse of width t_p (=10 ns) as a function of the excitation intensity using the theory of Ansari and Szabo (in preparation).[2] The theory accounts for the effect of rotational diffusion within the excitation pulse and contains two adjustable parameters: a generalized order parameter

[2] More detailed calculations showed no significant effects of pulse shape.

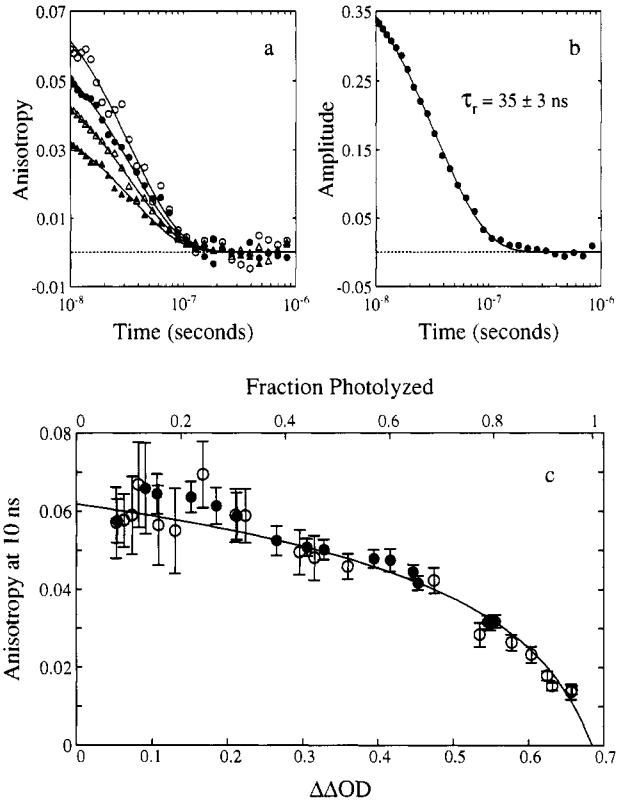

FIGURE 3: Decay and photolysis dependence of the average anisotropy. (a) Representative decay curves for the average anisotropy, $\bar{r}(t)$, calculated using eq 6, were obtained at the following levels of photolysis: 27% (open circles), 44% (filled circles), 66% (open triangles), and 81% (filled triangles). The continuous curves were obtained by fitting the first microsecond of the data with a single exponential having the same time constant (36 ns) at all levels of photolysis. (b) Singular value decomposition of the decay curves. The data are the first basis component of the SVD of the decay curves at all 16 levels of photolysis, and the continuous curve is the exponential fit to the data with a time constant of 35 ns. Prior to the SVD of the data, the individual anisotropy decay curves were weighted by the reciprocal of the noise in the curve. The noise was calculated as the sum of the squared residuals obtained in a polynomial fit to the data. (c) The average anisotropy (eq 6) at 10 ns (calculated from the exponential fit) is plotted as a function of the mean ΔΔOD [≡ΔOD(435 nm) − ΔOD(419 nm)] for the isotropically averaged spectra (eq 5) between 10 and 15 ns. Data for both sample concentrations were included in the figure (filled circles, 120 μM sample; open circles, 950 μM sample). The small difference in sample absorbance was accounted for by scaling the 950 μM data by a factor of 0.94. The continuous curve is a fit through the data points using the theory described in the text. The fit yielded 0.90 ± 0.04 for S, the generalized order parameter, and 0.69 ± 0.02 for the ΔΔOD at infinite laser intensity from which the fraction photolyzed (upper abscissa) for the combined data set was calculated.

and the value of the spectral amplitude at infinite laser intensity.

The anisotropy after the pulse is given by

$$r(t > t_p) = \frac{S}{10}\frac{a_2(t_p)}{1 - a_0(t_p)}\exp(-6D_r(t - t_p)) \quad (7)$$

where a_0 and a_2 depend upon the excitation intensity. The parameter $a_0(t_p)$ represents the fraction of hemes that have a ligand bound at the end of the pulse, and $a_2(t_p)$ is proportional to the linear dichroism in the sample. S is the generalized order parameter of the heme as defined by Lipari and Szabo (1980) and is a measure of the amplitude of the internal motions of the heme that are much faster than rotational diffusion. D_r is the rotational diffusion constant of the hemoglobin molecule. In eq 7, t is the time delay from the beginning of the pulse. In applying this equation 5 ns was added to the experimental times. The values of a_0 and a_2

were calculated by numerically solving a system of coupled differential equations:

$$\frac{da_l(t)}{dt} = -l(l+1)D_r a_l(t) - \frac{2l+1}{2}\epsilon I \int_0^{\pi}[1 - SP_2(\cos\theta)]\sum_{l'} a_{l'}P_l(\cos\theta)P_{l'}(\cos\theta)\sin\theta\, d\theta \quad (8)$$

where P_l are the Legendre polynomials, ϵ is the extinction coefficient of the liganded heme at the excitation wavelength, I is the excitation intensity, θ is the angle between the transition moment direction of the heme and the polarization direction of the photolysis laser, and a_l are the coefficients that describe the anisotropic distribution of the liganded molecules as a sum of Legendre polynomials. Prior to the excitation pulse, the distribution is assumed to be isotropic with all hemes having a ligand bound; the initial values of the coefficients are therefore $a_0 = 1$ and $a_l = 0$ for $l > 0$. The coefficients a_0 and a_2 were evaluated as a function of the excitation intensity using eq 8 after the Legendre polynomial series was truncated to $l = 8$.

Since we did not have an accurate measure of the excitation intensity in each experiment we took the following approach: a_0 and a_2 were obtained by solving the system of equations defined in eq 8 for various values of the excitation intensity. Experimentally the fraction of hemes photolyzed in each experiment is defined as

$$1 - a_0 = \frac{\Delta\Delta OD_{iso}}{\Delta\Delta OD_{max}} \quad (9)$$

which is the ratio of the amplitudes at 10 ns of the isotropic spectra, $\Delta\Delta OD_{iso}$, and the amplitude at infinite laser power with all the hemes photolyzed, $\Delta\Delta OD_{max}$. The complete photolysis limit is rarely achieved in the laboratory. Without making any assumptions about the maximal degree of photolysis in our experiments, the parameters $\Delta\Delta OD_{max}$ and S were varied simultaneously in order to minimize the residuals between the experimental and theoretically calculated values of the anisotropy at 10 ns. Theoretical anisotropies were calculated from eq 7. To do so, the value of a_0 was obtained from eq 9 and the corresponding value of a_2 was obtained by interpolating on the values determined using eq 8. Using the rotational correlation time of 36 ns, the best least-squares fit to the data in Figure 3c gave an order parameter S of 0.90 ± 0.04 and a spectral amplitude $\Delta\Delta OD_{max}$ of 0.69.

Kinetics as a Function of the Degree of Photolysis. To investigate the kinetics of ligand rebinding and conformational changes without interference from photoselection effects, the isotropically averaged spectra were calculated from the spectra for the individual polarizations using eq 5. The results of the singular value decomposition of the isotropically averaged data at all time delays and levels of photolysis are shown in Figure 4. SVD of this data matrix produced only two significant basis spectra (U_1 and U_2), which have singular values of $s_1 = 16.1$ and $s_2 = 0.77$. The next highest singular value ($s_3 = 0.07$) is only 0.4% of the singular value for the largest component (s_1); while there is some time-correlated information in this component, it is too small for detailed analysis. Higher order components arose from instrumental artifacts such as baseline dispersion (U_4) or from noise (U_5 and all higher components) and exhibited only random time dependencies, as observed in V_4.

The first basis spectrum (U_1) is the average photoproduct minus HbCO spectrum and is very similar to an equilibrium deoxyHb minus HbCO spectrum. The second basis spectrum (U_2) represents the deviation from the average spectrum and

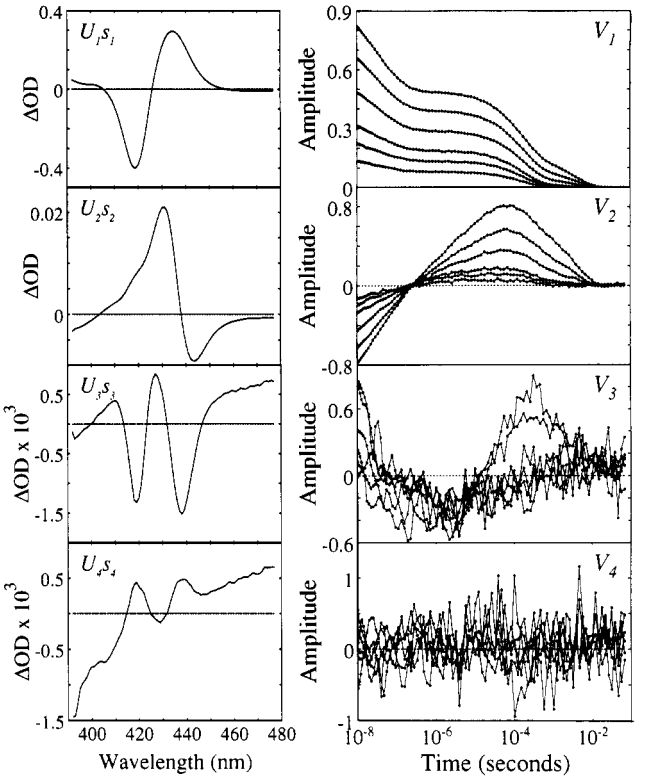

FIGURE 4: Singular value decomposition of the isotropically averaged data for the 16 levels of photolysis. The components with the four highest singular values are shown. The time courses for only 6 (13%, 22%, 31%, 48%, 65%, and 81%) of the 16 levels of photolysis are displayed in the V components. The V curves were normalized by setting the maximal amplitude of the V_1 curve at 81% photolysis equal to 0.81. The basis spectra were multiplied by the reciprocal of the scale factor used to normalize the V curves.

appears to be mainly a shift and intensity change of a deoxyHb spectrum. The fact that there is only a very small contribution of a deoxyHb minus HbCO difference spectrum to U_2 indicates that V_1 is an excellent approximation to the ligand rebinding curve. Information on the kinetics of the deoxyheme spectral changes is contained in V_2. The interpretation of V_2 is complex because it contains two contributions. One is a change in the deoxyheme spectrum, reflecting changes in the protein conformation (Murray et al., 1988b); the second is a decrease in the overall magnitude of the spectrum due to the depletion of deoxyhemes from ligand rebinding.

Initial examination of the ligand rebinding curves (V_1) in Figure 4 indicates that they have similar shapes between 10 ns and about 10 μs. At longer times the shapes are different because of different relative amplitudes of the two major bimolecular ligand rebinding phases. Differences in the kinetics of the deoxyheme spectral changes (V_2) appear earlier. The data in Figure 4 show that there is a proportionately much larger decrease in the magnitude of V_2 with decreasing degree of photolysis at 10 μs compared with 10 ns. Comparison of the residuals from a fit to the spectra at each time delay with a single average spectrum indicates that the spectra are very similar at all degrees of photolysis between 10 ns and 1 μs (Figure 5). In this time range all of the ligand rebinding is geminate. At 1 μs an abrupt increase occurs, indicating that the spectra at all levels of photolysis can no longer be described by a single average spectrum. At about 1 ms the deviations again fall within the noise level. On the basis of the results in Figure 5 we chose to make a more detailed comparison of the kinetics of ligand rebinding and deoxyheme spectral changes in the 10 ns–1 μs time range.

The data were compared by two methods. First, the kinetics were fitted with sums of exponentials and the dependencies

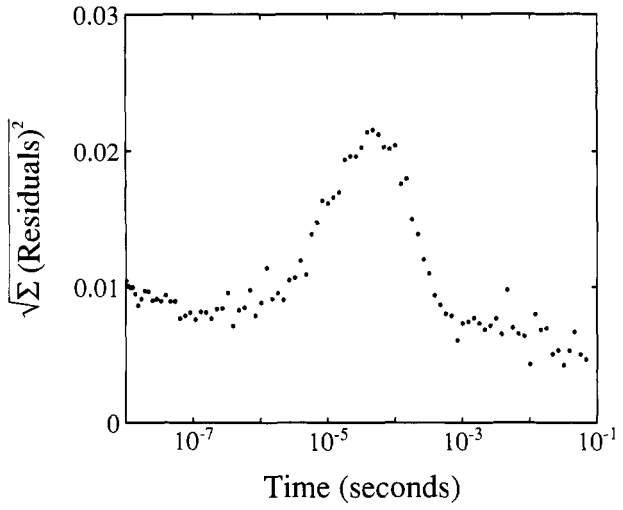

FIGURE 5: Comparison of the photolysis dependence of the isotropically averaged spectra as a function of the time delay. The square root of the sum of the squared residuals was calculated after fitting the isotropic spectra at all levels of photolysis for a particular time delay with the average spectrum obtained as the first component of the SVD of these spectra. The gradual slope in the data derives from noise contributions which decrease as the overall signal decays from ligand rebinding.

of the relaxation times and amplitudes on the degree of photolysis were examined. The use of exponentials assumes that the kinetics can be described by a system of coupled, linear first-order differential equations. The results in Figure 6a, obtained by fitting V_1 and V_2 simultaneously to obtain a set of relaxation rates at each degree of photolysis, show that the first three relaxation rates are independent of the degree of photolysis. To examine the dependence of the amplitudes of these three relaxations on the extent of photolysis, the entire set of V_1 and V_2 curves were fitted simultaneously with a single set of relaxation rates. The use of this procedure is necessary because the amplitudes of the relaxations are sensitive to the values of the relaxation rates. The ligand rebinding curve (V_1) can be well-fitted by two exponential relaxations in the 10 ns–1 μs time range; there is negligible rebinding in the third relaxation (Figure 6c). The curves describing the kinetics of the deoxyheme spectral changes (V_2), however, require three exponentials. The amplitudes of the submicrosecond relaxations for both V_1 and V_2 are linearly proportional to the fraction photolyzed. Thus, like the relaxation times, the fractional geminate rebinding and deoxyheme spectral changes are independent of the number of photodissociated ligands.[3]

The same result can be obtained much more easily and rapidly by using singular value decomposition to compare the kinetic curves (Figure 7). A very useful property of SVD is that it can be used to examine the similarity of a set of curves of any type in a model-independent manner, i.e., without assuming a functional form. The first two basis curves of the SVD of the ligand rebinding curves are shown in Figure 7b. The singular value of the second basis curve is only 0.2% of that of the first, indicating that all of the curves can be described by a single basis curve. That is, all of the ligand rebinding curves have the same shape. Therefore, the time constants

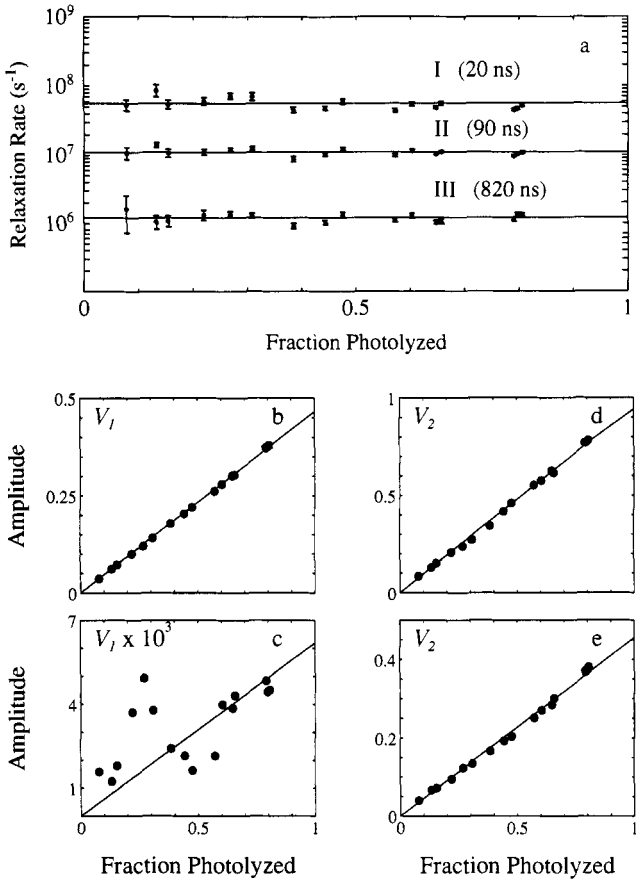

FIGURE 6: Comparison of the kinetics of ligand rebinding and deoxyheme spectral changes at different degrees of photolysis by a multiexponential analysis. (a) Photolysis dependence of the relaxation rate constants for the first three relaxations (I–III). The entire time courses (10 ns–70 ms) of the V_1 and V_2 curves were simultaneously fitted at each level of photolysis. Only five exponentials were required to fit the data at the lowest levels of photolysis, while seven were needed to adequately fit the more complex bimolecular kinetics at times greater than 1 μs in the higher photolysis experiments. The fit with a χ^2 of approximately 1–1.5 was chosen for data at each level of photolysis. The mean value of the relaxation rate is indicated by the horizontal line. (b–e) Photolysis dependence of the amplitudes obtained from a simultaneous exponential fit. The entire set of V_1 and V_2 curves were simultaneously fitted with a single set of relaxation rate constants. Seven exponentials were required to obtain an adequate fit to the set of isotropic ligand rebinding and deoxyheme spectral change kinetic progress curves. The absolute values of the amplitudes are plotted in panels b–e. The amplitudes have been normalized by the total ligand rebinding amplitude extrapolated to 100% photolysis. The amplitudes for the first two relaxations have been combined for both V_1 (panel b) and V_2 (panel d), since they were found to be highly anticorrelated and not uniquely determined by exponential modeling. Amplitudes for the third (820-ns) relaxation for V_1 and V_2 are shown in panels c and e, respectively. The lines are least-squares fits through the data points. The results of the exponential fit predict that 8% of the total ligand rebinding amplitude is not observed since it occurs at times shorter than the experimental resolution of 10 ns.

and *relative* amplitudes of the processes that make up the geminate rebinding progress curves are identical at all degrees of photolysis. The *absolute* amplitude of the fractional geminate rebinding is also independent of the degree of photolysis, as evidenced by the perfect linearity in the plot of the amplitude of the first basis curve versus fractional photolysis (Figure 7c).

The results of the SVD of the kinetic curves for the deoxyheme spectral changes are very similar (Figures 7d–f). These curves are very well represented by a single basis curve (the second basis component has a singular value which is only 1.7% of that of the first). Again, this result indicates that the processes contributing to these kinetics have the same time

[3] There is a suggestion of curvature in the plot for the 820-ns relaxation in Figure 6e, which is more evident in the 950 μM sample. In iron–cobalt hybrid hemoglobins, photodissociation of the carbon monoxide complex produced a small spectral change in the cobalt porphyrins with time constants of 1–2 μs (Hofrichter et al., 1985). These observations may represent some structural communication between subunits prior to the quaternary conformational change. An alternative interpretation is that the quaternary conformational change is multiexponential.

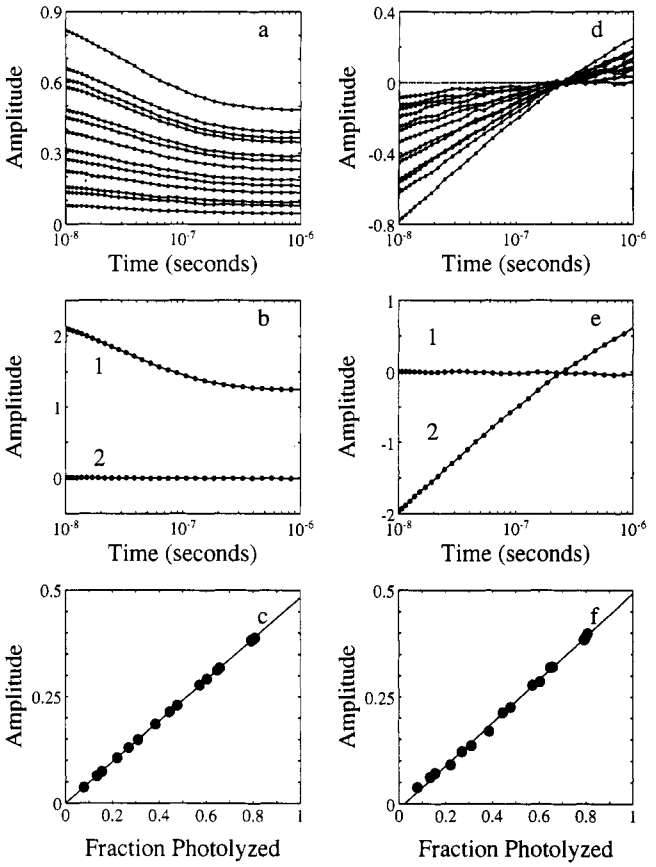

FIGURE 7: Comparison of the kinetics of ligand rebinding and deoxyheme spectral changes from 10 ns to 1 μs at different degrees of photolysis by singular value decomposition. Three of the curves at the highest fraction photolyzed have been deleted from the plot to simplify the figure. (a) Ligand rebinding curves (V_1). (b) First two basis curves (labeled 1 and 2) obtained from the singular value decomposition of all 16 ligand rebinding curves. The basis curves have been multiplied by their singular values. (c) Amplitude of basis curve 1 as a function of the fractional photolysis. (d) Deoxyheme spectral changes (V_2). (e) First two basis curves (1 and 2) from the singular value decomposition of all 16 deoxyheme spectral change progress curves. The basis curves have been multiplied by their singular values. (f) Amplitude of basis curve 1 as a function of the fractional photolysis. The set of V_1 and V_2 were normalized by setting the amplitude of the highest photolysis isotropic ligand rebinding curve at 10 ns equal to 0.81. The lines in panels c and f are least-squares fits through the data points, weighted by the reciprocal of the noise in the V_1 and V_2 curves. The noise was calculated as the sum of the squared residuals obtained in a polynomial fit to the data.

constants and *relative* amplitudes at all degrees of photolysis. Also, the *absolute* amplitude of the first basis curve scales linearly with the degree of photolysis (Figure 7f). As with geminate rebinding, then, the kinetics of the deoxyheme spectral changes are independent of the number of ligands photodissociated from the tetramer.

The comparison of the spectra at each time delay shown in Figure 5 indicates that the spectra are no longer the same after about 1 μs. In the multiexponential analysis the first relaxation after this time occurs at about 10 μs. Figure 8b shows that the amplitude for the deoxyheme spectral change associated with this relaxation is nonlinear in the degree of photolysis, indicating that this process involves some kind of communication between subunits. To compare these results with the predictions of the two-state allosteric model, the amplitudes were calculated as a function of the fraction of deoxyhemes (Figure 8). In this calculation it was assumed that the distribution of ligation states is binomial, that the spectral change is independent of the ligation state of the protein, and that the allosteric parameter c is the same for carbon monoxide and oxygen. Each ligation state shows a

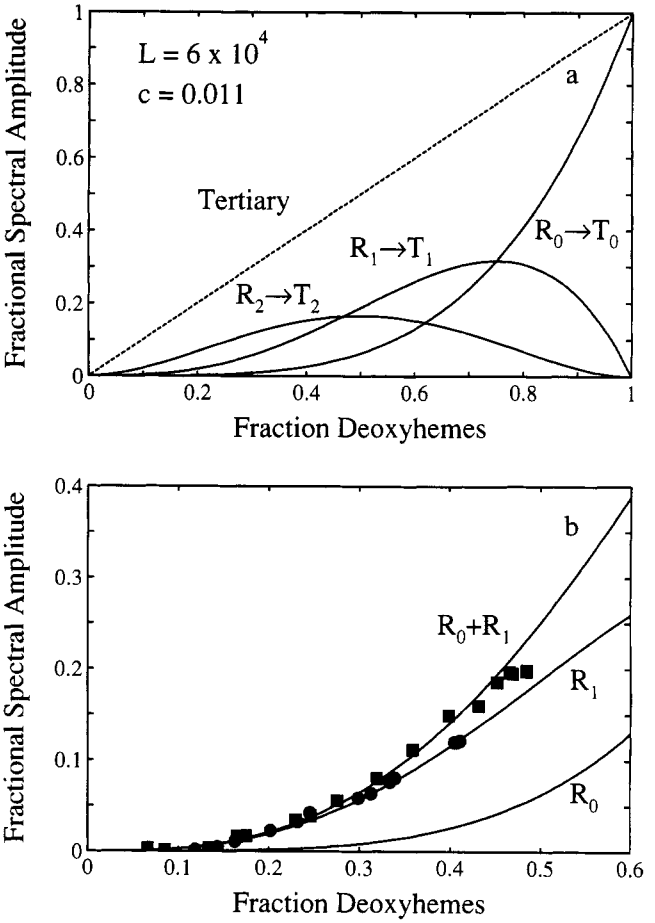

FIGURE 8: Amplitudes of the deoxyheme spectral changes associated with tertiary and quaternary protein conformational transitions. (a) The solid lines show the populations of the various ligation states of R-state hemoglobin tetramers predicted by the two-state MWC model to undergo a quaternary conformational transition. A binomial distribution of liganded species was assumed to be present prior to the quaternary conformational change (Hofrichter et al., 1991); the contribution of dimers was neglected in the analysis since the amplitudes for the 120 μM and 950 μM samples were indistinguishable (see panel b). The allosteric L, which defines the equilibrium constant for the R → T transition for the unliganded tetramer, was taken to be 6.0×10^4 (Eaton & Hofrichter, 1990). The parameter c, which is the ratio of the R- and T-state dissociation constants, was set at a value of 0.011. The dashed line shows that for a tertiary conformational relaxation the amplitude is linearly proportional to the fraction of deoxyhemes. (b) Comparison of the observed and predicted amplitudes for the deoxyheme spectral change associated with the 10-μs relaxation. The solid lines show the predicted amplitudes of the deoxyheme spectral change assuming that (1) only R_0 molecules switch to T_0, (2) only R_1 molecules switch to T_1, and (3) both R_0 and R_1 molecules switch to T-state molecules. Data for both sample concentrations were included in the figure (filled circles, 120 μM sample; filled squares, 950 μM sample). The experimental amplitudes were scaled by taking advantage of the observed linear relationship between these amplitudes and the ligand rebinding amplitude appearing in the T-state bimolecular rebinding phase at 4 ms. This linearity indicates that the population of deoxyhemes appearing in the T-state bimolecular rebinding phase are those molecules which have undergone a quaternary conformational transition during the 10-μs relaxation. The ratio of these amplitudes yields a spectral change amplitude per deoxyheme of 3.1 (in the amplitude units of Figure 4). This value corresponds to a $\Delta\epsilon$ at 430 nm of 15 $mM^{-1}\cdot cm^{-1}$ per deoxyheme switching from R to T.

characteristic dependence of the spectral amplitude on the fraction of deoxyhemes. The data agree with the theoretical curve where both unliganded and singly liganded tetramers switch to the quaternary T conformation in the 10-μs relaxation. Data obtained at higher temperatures where a larger fraction of deoxyhemes contribute to the quaternary transition as a result of decreased geminate rebinding also

follow the theoretical curve where both R_0 and R_1 molecules switch (Jones et al., unpublished results). There is insufficient precision in the data to resolve both rates and amplitudes for two relaxations in this time regime. However, there is a suggestion that the relaxation rates increase with increasing photolysis. Also, fits employing an additional relaxation for the R → T conformational change, in which the ratio of the two quaternary relaxation rates was fixed at various values between 1.5 and 4 and only the amplitudes for the additional relaxation were used as fitting parameters, indicated that the faster relaxation has a smaller amplitude. Both of these results suggest that the R → T conformational change for the unliganded molecule is faster than that of the singly liganded molecule.

DISCUSSION

The results presented here constitute the first systematic study of the time-resolved absorption spectra of human hemoglobin as a function of the degree of photolysis. The ultimate goal of this work is to develop a model that connects the kinetics of both geminate and bimolecular ligand rebinding to the kinetics of the protein conformational changes. In this paper we have the more limited objective of determining how geminate rebinding and conformational relaxation depend on the number of heme–CO complexes in a tetramer that have been photodissociated. It was clear from the early studies of Gibson with microsecond laser pulses (Sawicki & Gibson, 1976) and later work with nanosecond laser pulses (Hofrichter et al., 1983) that the kinetics of bimolecular carbon monoxide rebinding vary considerably with the degree of photolysis. There was, however, an indication in the nanosecond study, as well as in the recent study of Chiancone and Gibson (1989), that geminate rebinding of carbon monoxide is much less dependent on the degree of photolysis.[4] The present work represents a major extension of these earlier studies. The key to this study has been an improvement both in the instrumentation and in the measurement of the transient spectra with the polarization of the probe pulse both parallel and perpendicular to that of the photolysis pulse. Measurements with both polarizations not only permitted the calculation of isotropically averaged spectra, which are necessary for accurate determination of the populations of individual molecular species, but also yielded the optical anisotropy which provides information on the reorientational dynamics of the heme group. We first discuss the optical anisotropy results and then, using the isotropically averaged spectra, compare the kinetics of ligand rebinding and conformational changes at varying degrees of photolysis.

Optical Anisotropy. Photolysis with polarized light pulses induces a transient linear dichroism in the sample. The linear dichroism appears because molecules with their transition moments oriented more parallel to the electric vector of the photolysis pulse have a greater probability of absorption. The result is that these molecules are preferentially photodissociated ("photoselected"), producing a transient anisotropy in the orientational distribution of both photolyzed and unphotolyzed molecules. The fraction of photodissociated molecules will appear to be larger than the true value for observation with a light pulse polarized parallel to the photolysis pulse, while the opposite is true for perpendicular polarizations of the photolysis and probe pulses. The linear dichroism will decay to zero as the hemoglobin molecules rotationally diffuse to produce a random (isotropic) distribution.

The large effects of photoselection and rotational diffusion are shown in Figures 2 and 3. The apparent fraction of deoxyhemes immediately after photodissociation is greater for measurements with parallel polarizations (Figure 2) but becomes equal to the fraction measured with perpendicular polarizations after the linear dichroism disappears at about 200 ns. There are two principal contributions to the decay in the linear dichroism (Figure 2). One is the decrease in the overall difference spectrum due to geminate rebinding, which is complete at about 300 ns, and the second is the randomization of the molecular orientations by rotational diffusion. To eliminate the effect of geminate rebinding we calculate the average optical absorption anisotropy, defined by eq 6. Geminate rebinding is analogous to the depletion of the excited state population in polarized fluorescence experiments and, similarly, makes no contribution to the optical anisotropy.

The interesting quantities that can be obtained from the linear dichroism measurements are the decay time and the magnitude of the optical anisotropy evaluated prior to the overall rotational diffusion of the molecule. The anisotropy decay is well-fitted by a single exponential with a decay time of 36 ± 3 ns (Figure 3). As discussed elsewhere (Hofrichter et al., in preparation), the value predicted by hydrodynamic theory for a prolate ellipsoid with the dimensions of hemoglobin having a single layer of water bound to its surface is 33 ns.

To obtain the magnitude of the anisotropy prior to the onset of rotational diffusion we consider the data in Figure 3c. In this figure the anisotropies at 10 ns are plotted as a function of the overall isotropic spectral amplitude of the photoproduct. In the limit of vanishingly small intensity of the photolysis pulse, the measured anisotropy at 10 ns is between 0.06 and 0.07. The theoretical value for a perfect circular absorber in the absence of any heme reorientation at zero time, i.e., the limiting anisotropy, is 0.1 (which corresponds to $S = 1.0$ in eq 7). Having determined the rotational correlation time, we used the theoretical formalism of Ansari and Szabo to correct for the decreased anisotropy resulting from overall motion of the hemoglobin molecule during the photolysis pulse (eqs 7–9). The curve through the data in Figure 3c is the result of this theoretical calculation, which contains only two adjustable parameters, S and $\Delta\Delta OD_{max}$. S is a generalized order parameter which is a measure of the amplitude of the fluctuation in the orientation of the heme plane (Lipari & Szabo, 1980), while $\Delta\Delta OD_{max}$ is the overall isotropic spectral amplitude at 10 ns for infinite laser intensity. The value of S that best fits the data is 0.90 ± 0.04, which is significantly lower than 1.0, the value for a rigidly attached chromophore. There are three possible effects which could lower the order parameter: the presence of a z-polarized component (i.e., a component of the transition moment perpendicular to the heme plane) at either the photolysis or probe wavelengths, a subnanosecond change in the average orientation of the heme plane following photodissociation due to protein conformational relaxation, and subnanosecond fluctuations in the orientation of the heme group due to the internal dynamics of the protein. The largest contribution is most probably the internal dynamics of the protein (Ansari et al., in preparation).

A major advantage of measuring the optical anisotropy was that the extinction coefficients of the photoproduct could be accurately determined. A general problem in photolysis experiments is that it is difficult to determine the fraction of molecules that have been photodissociated, since the photoproduct extinction coefficients are generally unknown. To

[4] Chiancone and Gibson (1989) found that in the dimeric hemoglobin from *Scapharca inaequivalvis*, in which the hemes of each subunit are in direct contact, the rate of geminate rebinding of oxygen increases with the degree of photolysis, which they suggest indicates a communication between the two subunits of this molecule on a time scale of tens of nanoseconds or less.

determine this fraction it is therefore necessary to know the quantum yield and to have accurate measurements of the number of absorbed photons or, more practically, to make measurements as a function of laser intensity and extrapolate the data to infinite laser intensity. As can be seen from the fit to the data in Figure 3c, the optical anisotropy data have provided a sensitive method for determining the amplitude of the difference spectrum of the fully photolyzed molecule without knowing either the quantum yield or the laser intensity. In these experiments this amplitude, $\Delta\Delta OD_{max} = 0.69$, was determined with an uncertainty of less than 3%. As we shall see below, it is particularly important to accurately know the fraction of heme complexes that have been photodissociated, since both the thermodynamic and kinetic behavior of the hemoglobin molecule is determined by the number of hemes which have ligands bound.

Kinetics as a Function of the Degree of Photolysis. Both the kinetics of ligand rebinding and the kinetics of protein conformational changes as a function of the degree of photolysis can be investigated from the time-resolved optical absorption spectra. The ligand rebinding kinetics are given by the time course of the overall amplitude of the spectrum, as measured by the amplitude of the first basis spectrum in the singular value decomposition of the data. The information on the kinetics of conformational changes is contained in the time course of the amplitude of the second basis spectrum, which corresponds to a spectral change of the deoxyheme photoproduct. This spectral change is thought to arise from a displacement of the iron from the heme plane that is associated with the relaxation of the protein toward the conformation of deoxyhemoglobin at equilibrium (Murray et al., 1988b).

Several different methods were used to compare the kinetics of ligand rebinding and the kinetics of conformational changes at different degrees of photolysis. Visual inspection of the ligand binding curves in Figure 4 shows that the relative amplitudes of the two bimolecular phases at 190 μs and 4 ms are different at different degrees of photolysis. In contrast, the geminate rebinding phases appear to be identical at the different degrees of photolysis.

To establish an approximate time regime for comparing the similarity of the kinetics in more detail, the spectra at all degrees of photolysis were compared at each time delay. This comparison (Figure 5) shows that the spectra for every time delay are the same between about 10 ns and 1 μs and again at times longer than 1 ms. This result already implies that the ligand rebinding and conformational kinetics are independent of the degree of photolysis in the 10 ns–1 μs regime, and this is borne out by two additional, more detailed comparisons. In the first, the ligand rebinding and conformational progress curves were simultaneously fitted with a sum of exponentials, and both the rates and amplitudes for the three submicrosecond relaxations at about 20, 90, and 820 ns were found to be independent of the degree of photolysis (Figure 6). In the second, singular value decomposition of both the ligand rebinding and conformational relaxation progress curves showed only a single component and perfect linearity of the amplitude of this component with the degree of photolysis (Figure 7). The single-component description of the data indicates that the time constants and *relative* amplitudes are the same at all degrees of photolysis, while the linearity with the degree of photolysis indicates that the *absolute* amplitudes are independent of the degree of photolysis. Thus, all three methods of comparing the time-resolved spectra indicate that both the geminate rebinding and conformational relaxation kinetics are independent of the number

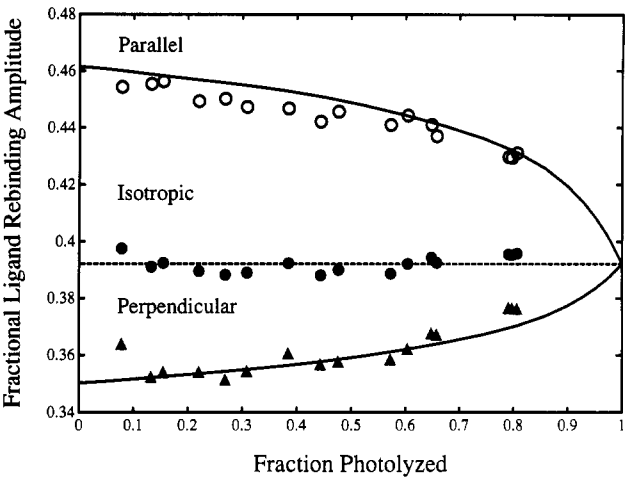

FIGURE 9: Effect of photoselection and rotational diffusion on the apparent ligand rebinding. The apparent fractional geminate rebinding amplitude between 10 ns and 1 μs, A, obtained from the V_1 amplitudes using $A = [V_1(10\text{ ns}) - V_1(1\ \mu\text{s})]/V_1(10\text{ ns})$ is plotted as a function of the fraction photolyzed. Data obtained using parallel (open circles) and perpendicular (filled triangles) polarizations of the photolysis and probe electric vectors is shown along with the isotropic geminate rebinding amplitude (filled circles). The solid lines through the polarized data are theoretically predicted values of the apparent fractional geminate rebinding amplitudes using the theory of photoselection (Ansari and Szabo, in preparation). The theoretical values are calculated using the following equations, where the apparent fraction of deoxyhemes is proportional to $f_\parallel(t) = 1 - a_0(t) + Sa_2(t)/5$ or $f_\perp(t) = 1 - a_0(t) - Sa_2(t)/10$ and the apparent fractional geminate rebinding amplitude at each level of photolysis is calculated from $A = [f_{\parallel,\perp}(10\text{ ns}) - f_{\parallel,\perp}(1\ \mu\text{s})]/f_{\parallel,\perp}(10\text{ ns})$. The values of $a_0(10\text{ ns})$ and $a_2(10\text{ ns})$ are obtained from eqs 8 and 9; the value of S, obtained from the fit to the anisotropy at 10 ns, is 0.90. Since 1 μs is long compared to the rotational correlation time (τ_r = 36 ns), $a_2(1\ \mu\text{s}) \approx 0$. Therefore, $f_\parallel(1\ \mu\text{s}) = f_\perp(1\ \mu\text{s}) = 1 - a_0(1\ \mu\text{s}) \approx [1 - a_0(10\text{ ns})](1 - \phi)$, where ϕ is the isotropic geminate rebinding amplitude at 1 μs. The value of ϕ is obtained from the mean of the isotropic amplitudes for all levels of photolysis, and is indicated as the dashed line through the isotropic data.

of ligands that have been photodissociated. Prior to 1 μs, then, there does not appear to be any structural communication between subunits, as measured by the deoxyheme spectral changes. There is also no functional communication, as measured by the kinetics of geminate rebinding.

We should emphasize two points concerning this result. First, it is model-independent. By using singular value decomposition to show that the shapes of the kinetic progress curves are identical and that their amplitudes are linear in the degree of photolysis, it has not even been necessary to assume a particular functional form. Furthermore, if only data from a single polarization were employed, the results would have been misleading. This is shown in Figure 9, where the apparent fraction of photodissociated ligands that geminately rebind between 10 ns and 1 μs is compared as a function of the degree of photolysis. For both parallel and perpendicular orientations of the polarization of the photolysis and probe pulses, the apparent geminate yield changes with increasing degree of photolysis, whereas the true geminate yield, as determined from the isotropically averaged data, is independent of the degree of photolysis.

When does intersubunit communication begin? Comparison of the spectra at a specific time delay (Figure 5) shows that differences begin to appear at about 1 μs. In the multiexponential fit of the ligand rebinding and conformational relaxation kinetics the first relaxation after 1 μs occurs at

about 10 μs.[5] This relaxation consists mainly of a deoxyheme spectral change with very little (1–2%) ligand rebinding. Figure 8b shows that, unlike the deoxyheme spectral changes in the submicrosecond time regime, the amplitude of the spectral change increases nonlinearly with the fraction of deoxyhemes present prior to this relaxation. This result indicates that the rates of the conformational change giving rise to the 10-μs relaxation depend on the number of ligands bound to the tetramer. That is, there is some kind of communication between subunits on this time scale.

To further interpret this result, we utilize the two-state allosteric model, which makes very specific predictions on how the spectral amplitude should scale with the fraction of deoxyhemes. Assuming a binomial distribution of ligands, we can use the thermodynamic parameters L and c, obtained from fitting oxygen binding curves under very similar solution conditions (Eaton & Hofrichter, 1990), to predict the spectral amplitudes. These parameters ($L = 6.0 \times 10^4$, $c = 0.011$) predict that prior to photodissociation fully liganded molecules are in the R conformation and that following photodissociation the entire population of unliganded, singly liganded, and doubly liganded molecules, and about 10% of the triply liganded molecules, will switch to the T conformation.[6] Each ligation state exhibits a characteristic dependence of the spectral amplitude on the fraction of deoxyhemes (Figure 8a).[7] In the absence of any competing processes, such as ligand rebinding or tertiary conformational relaxation within the R quaternary structure, these curves are potentially diagnostic of the ligation state of the tetramer undergoing the quaternary conformational change.

Comparison of these curves with the experimental data shows that the observed spectral amplitude is much too large to derive from a quaternary conformational change of the unliganded molecules only. The observed amplitudes are, however, consistent with the rates of the R to T conformational change for the unliganded and singly liganded molecules being almost the same. Marden et al. (1986) found no photolysis dependence of the R → T rates, and the dependence that we observe is marginal. The close correspondence of the $R_0 \rightarrow T_0$ and $R_1 \rightarrow T_1$ rates is expected from the linear free energy relation between the R → T rates and the equilibrium constants (Eaton et al., 1991). This relation indicates that singly liganded molecules switch from R to T about 3 times more slowly than unliganded molecules. Although the signal–to–noise in the present experiments is quite good, it is not possible to separate independent contributions from the $R_0 \rightarrow T_0$ and $R_1 \rightarrow T_1$ rates in the 10-μs relaxation. Attempts to fit the data with an additional relaxation do, however, suggest that the larger amplitude component has a longer relaxation time, which is consistent with the prediction of the linear free energy relation that $R_1 \rightarrow T_1$ is slower than $R_0 \rightarrow T_0$.

The preceding analysis suggests that there is no communication between subunits in hemoglobin in less than 1 μs and that the mechanism for the communication between subunits which occurs at later times is via the quaternary conformational change. The independence of geminate rebinding on the number of ligands bound to the tetramer is exactly what is expected for a two-state allosteric model. The essential feature of the two-state allosteric model for hemoglobin cooperativity is that ligand binding is noncooperative for both the R and T quaternary structures (Monod et al., 1965; Shulman et al., 1975). That is, the equilibrium constant, binding rate (including the rates of all the elementary steps that make up the binding rate, e.g., ligand entry or geminate rebinding), and dissociation rate are determined by the quaternary structure and are independent of the number of ligands that are already bound. The most convincing confirmation of this prediction for the T quaternary structure has come from the measurement of oxygen binding curves of single crystals (Mozzarelli et al., 1991). In these experiments the binding curve for the crystal, in which the T quaternary structure is stabilized by the intermolecular contacts, was found to be noncooperative. Comparable experiments have not yet been performed on crystals of hemoglobin in the R quaternary structure.

The question of cooperativity generated by subunit interaction in the absence of a quaternary conformational change is still a controversial issue. From an analysis of tetramer–dimer dissociation equilibria Ackers et al. (1992) have concluded that there is cooperativity within both the T and R quaternary structures. Ackers et al. (1992) quote a value for the Hill n of 1.0 for the binding of the third and fourth ligands to one of the doubly liganded species, $\alpha_1(\text{oxy})\beta_1(\text{deoxy})\alpha_2(\text{deoxy})\beta_2(\text{oxy})$, in the R conformation and a value of 1.2 for two of the doubly liganded species in the R conformation, $\alpha_1(\text{oxy})\beta_1(\text{deoxy})\alpha_2(\text{oxy})\beta_2(\text{deoxy})$ and $\alpha_1(\text{deoxy})\beta_1(\text{oxy})\alpha_2(\text{deoxy})\beta_2(\text{oxy})$. The fourth doubly liganded species, $\alpha_1(\text{oxy})\beta_1(\text{oxy})\alpha_2(\text{deoxy})\beta_2(\text{deoxy})$, is postulated to be in the T quaternary structure. The proposal that there is significant cooperativity within the R conformation is not supported by other work. Modified hemoglobins and hemoglobin mutants which are assumed to remain in the R quaternary structure at all saturations have been shown to exhibit noncooperative binding curves in solution (Imai, 1982).

It is possible to cast our results in terms which can be compared with these equilibrium studies. The observed geminate yield at a given fraction photolyzed, x, is given by $\phi_{obs}(x) = \sum f_i(x)\phi_i$ ($i = 0, 1, 2, 3$), where $f_i(x)$ is the fraction of deoxyhemes in tetramers having i ligands bound immediately after photolysis and ϕ_i is the geminate yield for that species. We therefore need to specify the values of ϕ_i for each of the partially liganded species. The results of this paper clearly show that all species remain in the R quaternary state throughout the geminate rebinding, so we are interested only in the results of Ackers et al. (1992) which are relevant to this quaternary state. The comparison is most straightforward if it is assumed that subunit interaction occurs on a time scale which is fast compared to geminate rebinding. In this case all tertiary interactions are fully relaxed and each R-state tetramer has already achieved its equilibrium conformation at the end of the photolysis pulse. The results summarized by Ackers et al. (1992) provide no information on the affinities of the unliganded and singly liganded species since both are present only in the T quaternary state at equilibrium. We will therefore assume that there is no cooperativity in binding the first two ligands to the R conformation.

Relative values for the geminate yields for the doubly and triply liganded species can be deduced from the apparent Hill

[5] A five-exponential fit to the data yielded a time constant of 20 μs for this relaxation, as reported previously at a single high photolysis level (Hofrichter et al., 1983, 1985). In the earlier experiments the signal-to-noise in the data did not warrant fitting the progress curves with more than five exponentials.

[6] In a two-state allosteric model the two bimolecular phases at 190 μs and 4 ms (Figure 3) correspond to binding to the R and T conformations, respectively (Sawicki & Gibson, 1976; Hofrichter et al., 1983; Marden et al., 1986). As the degree of photolysis decreases there is a decrease in the fraction of molecules that are thermodynamically more stable in the T conformation. Consequently, fewer tetramers switch from the R to the T conformation, and the relative amplitude of the slow (T-state) rebinding phase at 4 ms decreases.

[7] The dependence of the spectral amplitude on the fraction of deoxyhemes is only slightly altered if one assumes the correct (nonbinomial) distribution of ligation states that is introduced because of correlated probabilities of photodissociating hemes on the same tetramer (Hofrichter et al., 1991).

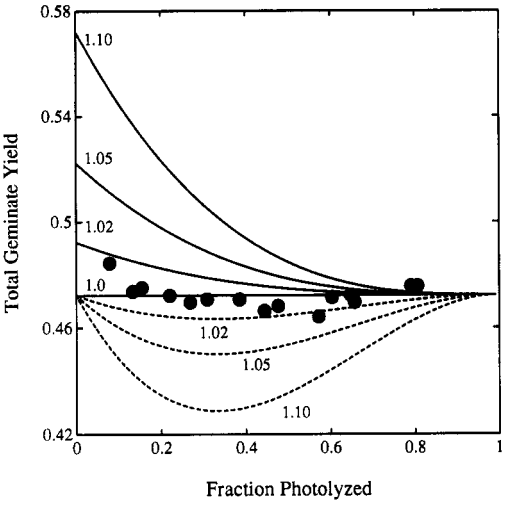

FIGURE 10: Comparison of predicted and observed geminate yield as a function of the fraction photolyzed. The experimental points are the sums of the ligand rebinding amplitudes for the first three relaxations at 20, 90, and 820 ns. The curves are calculated from eqs 10 (continuous lines) and 11 (dashed lines) and are the predicted amplitudes for varying degrees of cooperativity for binding of the third and fourth ligands to the tetramer as expressed by the Hill n indicated next to each curve. The distribution of liganded species immediately after photolysis is assumed to be binomial.

n values referred to above if it is assumed that all of the cooperativity in binding the last two ligands is manifested in the geminate yield. This assumption is supported by the finding that, for carbon monoxide, most of the cooperativity appears in the overall association rates (Szabo, 1978) and that all of the difference in the association rates may be accounted for by differences in the geminate yield (Murray et al., 1988a). If we treat ligand binding to the doubly liganded tetramer as binding to a cooperative dimer, the ratio of the intrinsic association constants for the third and fourth ligand binding steps is related to the Hill n by $r = n^2/(2 - n^2)$ (Szabo & Karplus, 1975). The simplest model that relates the geminate yield to the overall binding rate, k_{on}, and dissociation rates, k_{off}, gives the relations $k_{on} = k_{entry}\phi$ and $k_{off} = k_{break}(1 - \phi)$ (Henry et al., 1983; Murray et al., 1988a). The overall binding rate is the product of the rate of ligand entry into the protein and the probability of binding, while the overall dissociation rate is the product of the bond-breaking rate and the probability of ligand escape from the protein. ϕ_3 can then be written in terms of ϕ_2 as $\phi_3 = r\phi_2/[1 + \phi_2(r-1)]$. If the geminate yields ϕ_0, ϕ_1, and ϕ_2 are assumed to be identical, then the observed geminate yield, ϕ_{obs}, is given by

$$\phi_{obs}(x) = \frac{f_3(x)r\phi_2}{1 + \phi_2(r-1)} + [1 - f_3(x)]\phi_2 \qquad (10)$$

or if ϕ_0, ϕ_1, and ϕ_3 are assumed to be identical

$$\phi_{obs}(x) = \frac{[1 - f_2(x)]r\phi_2}{1 + \phi_2(r-1)} + f_2(x)\phi_2 \qquad (11)$$

The experimental geminate yields measured as a function of the degree of photolysis are compared with predicted values based on the above assumptions in Figure 10. While a more realistic calculation would need to take into account the fact that tertiary conformational relaxations are observed to occur on the same time scale as geminate rebinding, thereby reducing the effect of n on the geminate yield, it is clear that kinetic data of this type can potentially rule out n values in excess of about 1.02. If the tertiary interactions are fast compared to geminate rebinding, this result suggests that Ackers et al. (1992) may have considerably overestimated the cooperativity with which ligands bind to the R quaternary structure. The alternative possibilities that the rate of subunit interaction is too slow to produce cooperativity in geminate rebinding experiments or that cooperativity within the R conformation is manifested in the bond-breaking or ligand entry rates which do not alter the geminate yield cannot be ruled out. Exploration of these possibilities will require detailed modeling of the geminate and bimolecular kinetics. Such studies are currently in progress.

REFERENCES

Ackers, G. K., Doyle, M. L., Myers, D., & Daugherty, M. A. (1992) *Science 255*, 54–63.

Alpert, B., El Mohsni, S., Lindqvist, L., & Tfibel, F. (1979) *Chem. Phys. Lett. 64*, 11–16.

Chiancone, E., & Gibson, Q. H. (1989) *J. Biol. Chem. 264*, 21062–21065.

Duddell, D. A., Morris, R. J., & Richards, J. T. (1979) *J. Chem. Soc., Chem. Commun.*, 75–76.

Eaton, W. A., & Hofrichter, J. (1990) *Adv. Protein Chem. 40*, 63–279.

Eaton, W. A., Henry, E. R., & Hofrichter, J. (1991) *Proc. Natl. Acad. Sci. U.S.A. 88*, 4472–4475.

Friedman, J. M. (1985) *Science 228*, 1273–1280.

Friedman, J. M., & Lyons, K. B. (1980) *Nature (London) 284*, 570–572.

Henry, E. R., & Hofrichter, J. (1992) *Methods Enzymol. 210*, 129–192.

Hofrichter, J., Sommer, J. H., Henry, E. R., & Eaton, W. A. (1983) *Proc. Natl. Acad. Sci. U.S.A. 80*, 2235–2239.

Hofrichter, J., Henry, E. R., Sommer, J. H., Deutsch, R., Ikeda-Saito, M., Yonetani, T., & Eaton, W. A. (1985) *Biochemistry 24*, 2667–2679.

Hofrichter, J., Henry, E. R., Szabo, A., Murray, L. P., Ansari, A., Jones, C. M., Coletta, M., Falcioni, G., Brunori, M., & Eaton, W. A. (1991) *Biochemistry 30*, 6583–6598.

Imai, K. (1982) *Allosteric Effects in Hemoglobin*, Cambridge University Press, Cambridge, England.

Lipari, G., & Szabo, A. (1980) *Biophys. J. 30*, 489–506.

Lyons, K. B., & Friedman, J. M. (1982) in *Hemoglobin and Oxygen Binding* (Ho, C., Eaton, W. A., Collman, J. P., Gibson, Q. H., Leigh, J. S., Margoliash, E., Moffat, K., & Scheidt, W. R., Eds.) pp 333–338, Elsevier/North-Holland, Amsterdam.

Marden, M. C., Hazard, E. S., & Gibson, Q. H. (1986) *Biochemistry 25*, 7591–7596.

Monod, J., Wyman, J., & Changeux, J.-P. (1965) *J. Mol. Biol. 12*, 88–118.

Mozzarelli, A., Rivetti, C., Rossi, G. L., Henry, E. R., & Eaton, W. A. (1991) *Nature 351*, 416–419.

Murray, L. P., Hofrichter, J., Henry, E. R., Ikeda-Saito, M., Kitagishi, K., Yonetani, T., & Eaton, W. A. (1988a) *Proc. Natl. Acad. Sci. U.S.A. 85*, 2151–2155.

Murray, L. P., Hofrichter, J., Henry, E. R., & Eaton, W. A. (1988b) *Biophys. Chem. 29*, 63–76.

Perutz, M. F. (1968) *J. Cryst. Growth 2*, 54–56.

Perutz, M. F. (1989) *Q. Rev. Biophys. 22*, 139–237.

Sassaroli, M., & Rousseau, D. L. (1987) *Biochemistry 26*, 3092–3098.

Sawicki, C. A., & Gibson, Q. H. (1976) *J. Biol. Chem. 251*, 1533–1542.

Schroeder, W. A., & Huisman, T. H. J. (1980) *The Chromatography of Hemoglobin*, Marcel Dekker, Inc., New York.

Shulman, R. G., Hopfield, J. J., & Ogawa, S. (1975) *Q. Rev. Biophys. 8*, 325–420.

Szabo, A. (1978) *Proc. Natl. Acad. Sci. U.S.A. 75*, 2108–2111.

Szabo, A., & Karplus, M. (1975) *Biochemistry 14*, 931–940.